

# Dynamic response of breast tumor oxygenation to hyperoxic respiratory challenge monitored with three oxygen-sensitive parameters

Yueqing Gu, Vincent A. Bourke, Jae G. Kim, Anca Constantinescu, Ralph P. Mason, and Hanli Liu

The simultaneous measurement of three oxygen-sensitive parameters [arterial hemoglobin oxygen saturation ( $\text{SaO}_2$ ), tumor vascular-oxygenated hemoglobin concentration ( $[\text{HbO}_2]$ ), and tumor oxygen tension ( $\text{pO}_2$ )] in response to hyperoxic respiratory challenge is demonstrated in rat breast tumors. The effects of two hyperoxic gases [oxygen and carbogen (5%  $\text{CO}_2$  and 95%  $\text{O}_2$ )] were compared, by use of two groups of Fisher rats with subcutaneous 13762NF breast tumors implanted in pedicles on the foreback. Two different gas-inhalation sequences were compared, i.e., air-carbogen-air-oxygen-air and air-oxygen-air-carbogen-air. The results demonstrate that both of the inhaled, hyperoxic gases significantly improved the tumor oxygen status. All three parameters displayed similar dynamic response to hyperoxic gas interventions, but with different response times: the fastest for arterial  $\text{SaO}_2$ , followed by biphasic changes in tumor vascular  $[\text{HbO}_2]$ , and then delayed responses for  $\text{pO}_2$ . Both of the gases induced similar changes in vascular oxygenation and regional tissue  $\text{pO}_2$  in the rat tumors, and changes in  $[\text{HbO}_2]$  and mean  $\text{pO}_2$  showed a linear correlation with large standard deviations, which presumably results from global versus local measurements. Indeed, the  $\text{pO}_2$  data revealed heterogeneous regional response to hyperoxic interventions. Although preliminary near-infrared measurements had been demonstrated previously in this model, the addition of the  $\text{pO}_2$  optical fiber probes provides a link between the noninvasive relative measurements of vascular phenomena based on endogenous reporter molecules, with the quantitative, albeit, invasive  $\text{pO}_2$  determinations. © 2003 Optical Society of America  
*OCIS codes:* 170.1470, 170.3660, 170.4580, 120.3890, 120.1880, 230.2090.

## 1. Introduction

It is widely recognized that hypoxic regions in solid tumors may limit the efficacy of nonsurgical therapy, including radiotherapy, photodynamic therapy, and chemotherapy.<sup>1-4</sup> Many adjuvant interventions have been tested, including simple strategies such as breathing hyperoxic gases.<sup>5-7</sup> However, a meta-analysis of some 10,000 patients showed only a modest benefit, and this benefit was restricted to specific tumor types.<sup>8</sup> It is thought that the failure of such interventions was largely due to the inability to iden-

tify those patients who would benefit. Indeed, there is growing emphasis on tailoring therapy to the individual characteristics of each patient's tumor. Furthermore, carbogen (5%  $\text{CO}_2$  and 95%  $\text{O}_2$ ) and oxygen have been used on experimental tumors in animals as well as on clinical trials in patients for many years.<sup>9,10</sup> But the therapeutic benefits of the two kinds of respiratory hyperoxic gases are diverse, depending on the tumor types and individuals.<sup>11-13</sup> Accordingly, accurate assessment of tumor oxygenation at various stages of tumor growth and in response to interventions may provide a better understanding of tumor development and may serve as a prognostic indicator for treatment outcome, potentially allowing therapy to be tailored to individual characteristics.

Various techniques have been developed to measure oxygen tension ( $\text{pO}_2$ ) or vascular oxygenation of tumors.<sup>14</sup> Many methods are invasive, and those requiring biopsy preclude dynamic investigations. Optical techniques based on light absorption of endogenous chromophores, e.g., near-infrared (NIR)

Y. Gu, J. G. Kim, and H. Liu (Hanli@uta.edu) are with the Biomedical Engineering Program, The University of Texas at Arlington, Arlington, Texas 76019. V. A. Bourke, A. Constantinescu, and R. P. Mason are with the Department of Radiology, University of Texas Southwestern Medical Center, Dallas, Texas 75390.

Received 8 September 2002; revised manuscript received 15 January 2003.

0003-6935/03/162960-08\$15.00/0

© 2003 Optical Society of America

spectroscopy of oxygenated and deoxygenated hemoglobin, are entirely noninvasive and allow real-time monitoring of tumor vascular oxygenation.<sup>15–17</sup> However, NIR has limited spatial resolution, and it remains to be determined whether vascular oxygenation is related to therapeutic outcome. Hitherto, quantitative  $pO_2$  has been shown to have prognostic value,<sup>18–21</sup> but  $pO_2$  represents a balance between oxygen delivery and consumption. Thus, we seek to explore the interplay of vascular and tissue oxygenation. Electrodes have been used widely to study tumor oxygen dynamics with respect to interventions,<sup>22–24</sup> but they are generally limited to a single location and small probes can be fragile. We have ourselves recently shown a correlation between  $pO_2$  and  $\Delta HbO_2$  in some tumors, but we noted distinct heterogeneity, and thus, the global NIR measurements were not always related to local  $pO_2$ .<sup>25</sup> Multiple fiber-optic probes may be inserted into a tumor,<sup>26–28</sup> and we have now investigated correlation between NIR measurements and multiple (three) simultaneous  $pO_2$  measurements.

We now report simultaneous measurements of three oxygen-related parameters, i.e., arterial hemoglobin oxygen saturation,  $SaO_2$ ; tumor oxygenated hemoglobin concentration,  $[HbO_2]$ ; and tumor oxygen tension,  $pO_2$ , to assess dynamic responses of rat breast tumors to hyperoxic gases. Changes in tumor vascular  $[HbO_2]$  were measured by NIR spectroscopy (NIRS) using a photon-migration, frequency-domain device; changes in regional  $pO_2$  were monitored by a fluorescence-quenched, oxygen-sensing, fiber-optic system (FOXY); the arterial  $SaO_2$  values were recorded with a fiber-based, pulse oximeter.

## 2. Materials and Methods

### A. Near-Infrared Spectroscopy System for Measurement of Changes in $[HbO_2]$

NIR light (700 to 900 nm) has considerable tissue penetration depth (several centimeters) and permits *in vivo* sampling of large tissue volumes (e.g., human breast, brain, skeletal muscle, or tumors), since photon transport in tissue is dominated by scattering rather than by absorption. Absorption of NIR light by the oxygenated and the deoxygenated hemoglobin chromophores may be used to determine hemoglobin oxygenation and blood concentration changes. As described in detail previously,<sup>16,25</sup> a homodyne frequency-domain system (NIM, Philadelphia, Pennsylvania) was used to monitor the global changes in oxygenated and deoxygenated hemoglobin concentrations,  $\Delta[HbO_2]$  and  $\Delta[Hb]$ , respectively, in rat breast tumors in response to variations in inhaled gas. Briefly, the light from two NIR laser diodes (758 nm and 785 nm) was coupled into a bifurcated fiber bundle and illuminated on the tumor, and the transmitted light was collected and propagated to a photomultiplier tube (Fig. 1). The fiber bundles were placed on the surface of the tumors in a transmittance mode parallel to the body of the rat. The fiber tips touched firmly on the skin (without com-

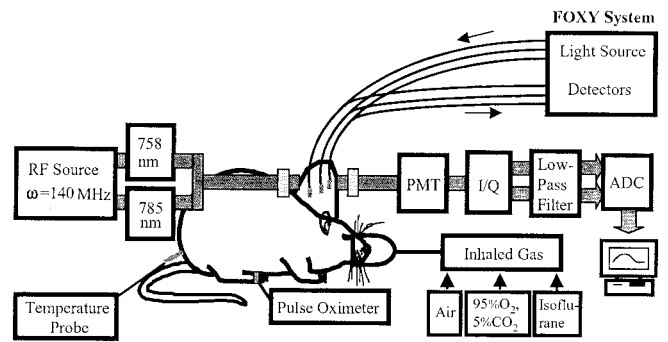


Fig. 1. Experimental setup for simultaneous oximetry. The 3-mm-diameter fiber bundles of the NIRS system deliver and detect the laser light through the tumor in transmittance geometry. PMT represents a photomultiplier tube. I/Q is an in-phase and quadrature phase demodulator for retrieving amplitude and phase information. The FOXY system comprises three fiber-optic oxygen-sensing probes that are inserted into different regions of the tumor. The pulse oximeter probe is placed on the hind foot of the rat.

pression) in the middle parts of the tumors, providing optimal geometry to interrogate deep tumor tissue.

Based on modified Beer–Lambert’s law,<sup>29</sup> changes in oxygenated and deoxygenated hemoglobin concentrations,  $\Delta[HbO_2]$  and  $\Delta[Hb]$ , due to respiratory intervention were derived from the measured amplitudes at the two wavelengths and calculated with the following equations<sup>25</sup>:

$$\Delta[HbO_2] = \frac{-10.63 \log\left(\frac{A_B}{A_T}\right)^{758} + 14.97 \log\left(\frac{A_B}{A_T}\right)^{785}}{d}, \quad (1)$$

$$\Delta[Hb] = \frac{8.95 \log\left(\frac{A_B}{A_T}\right)^{758} - 6.73 \log\left(\frac{A_B}{A_T}\right)^{785}}{d}, \quad (2)$$

where  $A_B$  and  $A_T$  are the baseline and transient amplitudes measured from the NIR system, respectively;  $d$  is the source–detector separation; the unit for both  $\Delta[HbO_2]$  and  $\Delta[Hb]$  is millimolar per differential path-length factor (DPF); and the DPF is for tumor tissues. As demonstrated in our previous study, normalization of  $\Delta[HbO_2]$  and  $\Delta[Hb]$  to their maximal values can eliminate the effects of  $d$  and DPF on the results.<sup>25</sup>

### B. Fiber-Optic Oxygen-Sensing System for Measurement of Changes in $pO_2$

Regional  $pO_2$  in tumors was monitored with a multichannel, fiber-optic, oxygen-sensing system (FOXY, Ocean Optics, Inc., Dunedin, Florida).<sup>30</sup> Three fluorescence-quenched, optical fiber probes (AL300, tip diameter 410  $\mu\text{m}$ ) were inserted into different regions of the tumors (Fig. 1). Probes were positioned so that at least one was in a poorly oxygenated region (low baseline  $pO_2$ ) and at least one in a well-oxygenated region (high baseline  $pO_2$ ). If necessary,

the probes were gently moved through the tumor until such diverse regions were located. In some cases, the mean  $pO_2$  derived from the three individual measurements is presented. Although this is a commercial system, few details have been published previously,<sup>31</sup> and no applications to *in vivo* tumor oximetry have been published to our knowledge. Light from a pulsed blue LED (475 nm) was coupled into one branch of a bifurcated optical fiber bundle and propagated to the probe tip. The distal end of the probe is coated with a thin layer of a hydrophobic solgel material, where an oxygen-sensing ruthenium complex is effectively trapped. Illumination of the ruthenium complex causes fluorescence at  $\sim 600$  nm. If the excited ruthenium complex encounters an oxygen molecule, the excess energy is transferred to the oxygen molecule in a nonradiative transition, decreasing or quenching the fluorescence signal. The degree of quenching correlates with the oxygen concentration, and hence,  $pO_2$ .

The fluorescence response of the ruthenium crystal complex is highly temperature dependent, so to accomplish probe calibration it was necessary to stream gases of known oxygen concentrations (100%, 20.9%, 10%, 2%, and 0%) through a cylindrical water jacket heated to 37 °C. Calibration curves were automatically calculated by means of the vendor-supplied software, with the second-order, polynomial calibration:

$$\frac{I_0}{I} = 1 + K_1[O] + K_2[O]^2 \quad (3)$$

where,  $I_0$  is the fluorescence intensity at zero oxygen concentration (nitrogen),  $I$  is the measured intensity of fluorescence at a pressure of oxygen,  $[O]$  represents the oxygen concentration (related to  $pO_2$ ),  $K_1$  and  $K_2$  are the first- and the second-order coefficients and are automatically supplied by the curve-fitting routine from the calibration measurements.

#### C. Pulse Oximeter for Measurement of Arterial $S_aO_2$

Arterial  $S_aO_2$  of the breast-tumor-bearing rats was also monitored with a fiber-optic pulse oximeter (Nonin Medical, Inc., Plymouth, Minnesota) placed on the hind foot of the rats. The system consisted of two optical fibers used for delivering and receiving the light. The tips were placed on either side of the foot in transmission mode.

#### D. Animal Model

Mammary adenocarcinomas 13762NF (originally obtained from the Division of Cancer Therapeutics, NIH, Bethesda, Maryland) were implanted in skin pedicles<sup>32</sup> on the foreback of adult female Fisher 344 rats ( $\sim 150$  g). Once the tumors reached 1–2 cm diameter, rats were anesthetized with 150- $\mu$ l ketamine hydrochloride (100 mg/ml, i.p.) and maintained under general gaseous anesthesia with 1.3% isoflurane in air (1 dm<sup>3</sup>/min). Body temperature was maintained at 37 °C by a warm water blanket. Tumors were shaved to improve optical contact for transmitting NIR light. The tumor diameters along the

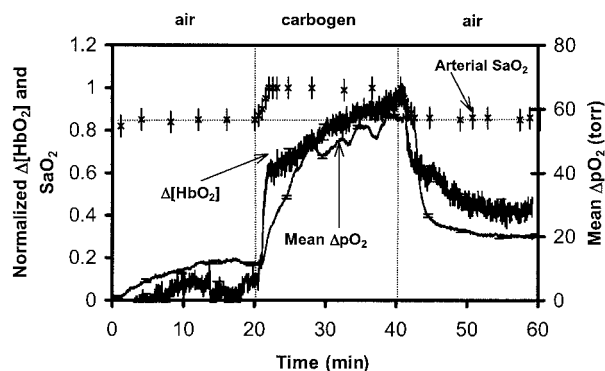


Fig. 2. Time profile of the three oxygen-sensitive parameters, i.e., the normalized changes of tumor  $\Delta[HbO_2]$ , the mean changes of tumor  $\Delta pO_2$ , and the arterial  $S_aO_2$  with respect to carbogen breathing in a representative 13762NF rat breast tumor (No. 1, 3.2 cm<sup>3</sup>).

three major orthogonal axes ( $a$ ,  $b$ ,  $c$ ) were measured with calipers and volume estimated with an ellipsoid approximation with the formula:  $V = (\pi/6)(abc)$ .

Two groups of rats ( $n = 7$  in each group) were used to compare the effects of carbogen and oxygen on vascular oxygenation of breast tumors. Group 1 experienced the gas-inhalation sequence of air–carbogen–air–oxygen–air. Group 2 was exposed to the reverse sequence of air–oxygen–air–carbogen–air. Each gas was maintained for 20 min. In addition, the FOXY  $pO_2$  probes were applied to five rats from Group 1, and the dynamics of the three oxygen-related parameters were measured simultaneously.

### 3. Results

#### A. Dynamic Responses of Three Oxygen-Related Parameters to Carbogen Intervention

Typical time profiles of the normalized  $\Delta[HbO_2]$ , mean  $\Delta pO_2$ , and  $S_aO_2$  in response to carbogen intervention are shown for a representative 13762NF breast tumor (No. 1, 3.2 cm<sup>3</sup>) in Fig. 2. When the inspired gas was switched from air to carbogen, the  $S_aO_2$  readings increased rapidly and significantly from the baseline value of 85% to the maximum of 100% within 2.5 minutes ( $p < 0.0001$ ). The normalized  $\Delta[HbO_2]$  showed a sharp initial rise in the first minute ( $p < 0.0001$ ) followed by a slower, gradual, but further significant increase over the next 19 min ( $p < 0.001$ ). Mean  $\Delta pO_2$  increased rapidly by approximately 50 Torr within 8 min ( $p < 0.0005$ ) and also continued a slower and gradual increase over the next 12 min ( $p < 0.005$ ). Return to breathing air produced a significant decline for all three signals ( $p < 0.0001$ ).

$S_aO_2$  and  $pO_2$  displayed a single-phase dynamic behavior in response to carbogen intervention, whereas  $\Delta[HbO_2]$  showed an apparent biphasic response. These dynamics may be characterized by time constants of a single-exponential response. For the tumor in Fig. 3,  $S_aO_2$  had the fastest response, with a time constant of  $\tau(S_aO_2) = 1.1 \pm 0.2$  min ( $R =$

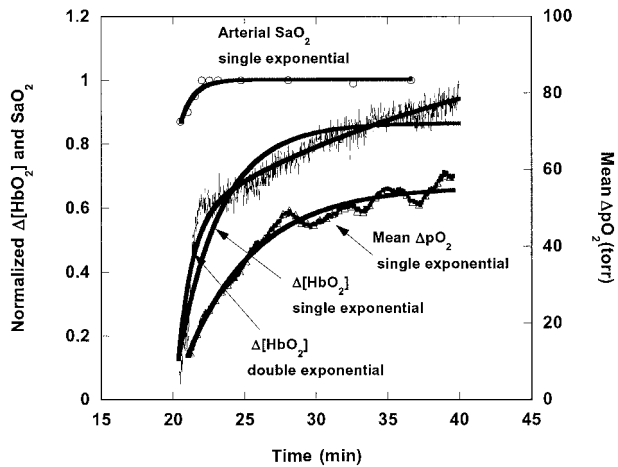


Fig. 3. Dynamic responses of the three oxygen-sensitive parameters to carbogen intervention in a rat breast tumor (No. 1, 3.2 cm<sup>3</sup>). Single-exponential curve fitting yielded  $SaO_2 = 0.204\{1 - \exp[-(t - 20.02)/1.1]\} + 0.85$  ( $R = 0.93$ ),  $\Delta[HbO_2] = 0.655\{1 - \exp[-(t - 20.36)/2.59]\} + 0.125$  ( $R = 0.89$ ), and  $\Delta pO_2 = 42.68\{1 - \exp[-(t - 21.01)/4.56]\} + 16.66$  ( $R = 0.98$ ); biexponential fitting resulted in  $\Delta[HbO_2] = 0.373\{1 - \exp[-(t - 20.36)/0.61]\} + 0.648\{1 - \exp[-(t - 20.36)/21]\}$  ( $R = 0.97$ ).

0.93), followed by  $[HbO_2]$  with  $\tau(\Delta[HbO_2]) = 2.59 \pm 0.06$  min ( $R = 0.89$ ), whereas  $\Delta pO_2$  yielded the slowest response  $\tau(\Delta pO_2) = 4.56 \pm 0.06$  min ( $R = 0.98$ ). Time constants for Group 1 are listed in Table 1. In every case  $\tau(SaO_2) < \tau(\Delta[HbO_2]) < \tau(\Delta pO_2)$ , based on the single-exponential fitting. No apparent relation between the time constant and the tumor volume was observed.

It is clear that the response of  $\Delta HbO_2$  is not well represented by a single exponential, and thus, a double-exponential expression with two time constants,  $\tau_1$  and  $\tau_2$ , was also used (Fig. 3). Comparison between the biexponential fitting for  $\Delta[HbO_2]$  and the single-exponential results for both  $SaO_2$  and  $\Delta pO_2$  in the first five rat tumors (Table 1) shows that the time constants of  $SaO_2$  ( $\sim 1.2 \pm 0.4$  min) are similar to those of the first phase of  $\Delta[HbO_2]$  ( $\sim 0.5 \pm 0.2$  min), whereas the second phase is longer and highly vari-

able ( $\sim 14 \pm 11$  min). No significant correlations were found between any of the time constants in Table 1.

Time delay,  $t_d$ , between the time when the gas intervention was initiated and the time when the changes in signals were detected, reveals another difference among the three oxygen-sensitive parameters. For tumor 1 (Fig. 2), the  $SaO_2$  signal was the first to respond to the intervention. Change in  $\Delta[HbO_2]$  was observed 30 s later with  $t_d = 30$  s, followed by changes in  $\Delta pO_2$  another 30 s later ( $t_d = 60$  s). Similarly, when the gas was returned from carbogen to air, the  $SaO_2$  signal decreased immediately, followed by declines in  $\Delta[HbO_2]$  and in  $\Delta pO_2$  with  $t_d$  of 30 and 120 s later, respectively. As expected, changes in  $SaO_2$  always preceded  $\Delta HbO_2$ , and  $\Delta pO_2$  occurred last for all tumors.

#### B. Comparison of the Effects of Carbogen and Oxygen Intervention on Tumor Oxygenation

Switching from air breathing to carbogen or oxygen produced similar changes in  $\Delta HbO_2$  [Fig. 4(a)]. However, the time course was substantially different, requiring a biphasic exponential fit for carbogen, but a single exponential for oxygen [Fig. 4(b)]. For the seven tumors in Group 1, there was no significant difference ( $p > 0.3$ ) in the maximum magnitude of  $\Delta[HbO_2]$  caused by carbogen or oxygen interventions [Fig. 4(c)].

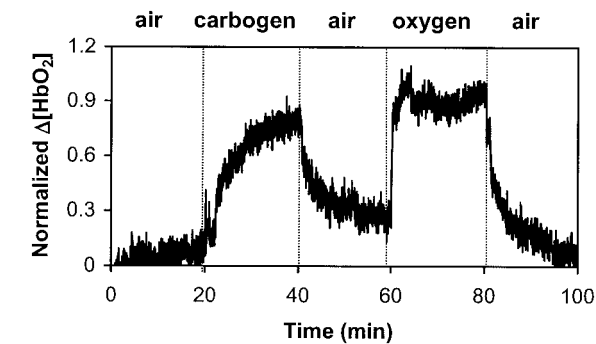
To examine the possible effect of preconditioning required that Group 2 experience a reversed gas intervention, with exposure to oxygen prior to carbogen [Fig. 5(a)]. In this case, the time constants of the normalized tumor vascular  $\Delta[HbO_2]$  were now similar for both gas challenges: indeed, for six of seven tumors, carbogen no longer induced the biphasic behavior. Figure 5(b) shows that changes in  $(\Delta HbO_2)_{max}$  were similar to those in Group 1, and again, the two gases did not produce significantly different response in  $(\Delta HbO_2)_{max}$ . This is emphasized for both Groups 1 and 2 by a strong linear correlation (slope  $\cong 1.16$ ) between the  $\Delta[HbO_2]_{max}$  values observed in response to each of the two con-

Table 1. Time Constants of  $SaO_2$ ,  $\Delta[HbO_2]$ , and  $\Delta pO_2$  Response to Carbogen and Oxygen Intervention in the Breast Tumors<sup>a</sup>

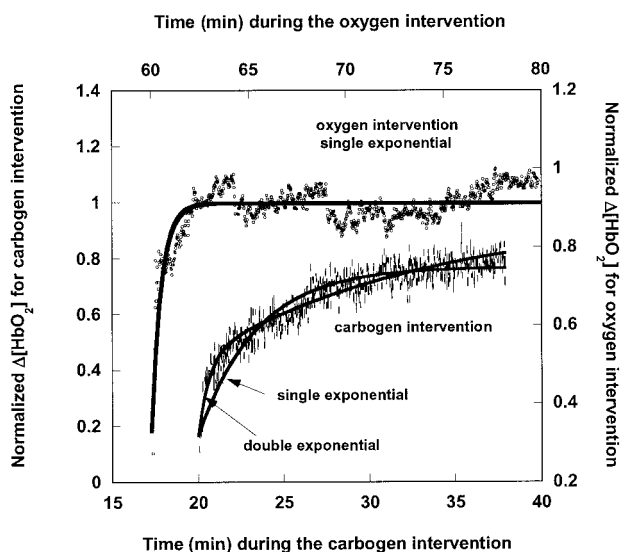
Breast Tumors Volume (cm <sup>3</sup> )	Single-Exponential Fitting of $SaO_2$ , $\Delta[HbO_2]$ and $\Delta pO_2$ (Carbogen Intervention)						Double-Exponential Fitting for $\Delta[HbO_2]$ (Carbogen Intervention)			Single-Exponential Fitting of $\Delta[HbO_2]$ (O <sub>2</sub> Intervention)	
	$SaO_2$		$\Delta[HbO_2]$		$\Delta pO_2$		$\tau_1$ (min)	$\tau_2$ (min)	$R$	$\tau$ (min)	$R$
	$\tau$ (min)	$R$	$\tau$ (min)	$R$	$\tau$ (min)	$R$					
No. 1 (3.2)	1.1 ± 0.2	0.93	2.59 ± 0.06	0.89	4.56 ± 0.04	0.98	0.61 ± 0.03	21 ± 3	0.97	0.35 ± 0.01	0.92
No. 2 (3.0)	1.6 ± 0.2	0.98	3.40 ± 0.07	0.91	4.6 ± 0.1	0.82	0.62 ± 0.06	11 ± 1	0.96	0.51 ± 0.01	0.91
No. 3 (4.6)	1.2 ± 0.2	0.97	2.12 ± 0.06	0.76	2.26 ± 0.02	0.98	0.6 ± 0.1	37 ± 3	0.96	1.52 ± 0.02	0.89
No. 4 (2.6)	1.9 ± 0.3	0.98	2.68 ± 0.05	0.93	3.5 ± 0.1	0.86	0.12 ± 0.02	5.2 ± 0.1	0.98	1.71 ± 0.03	0.94
No. 5 (5.6)	0.8 ± 0.2	0.91	2.68 ± 0.05	0.74	4.51 ± 0.02	0.99	0.17 ± 0.03	12.5 ± 0.6	0.99	5.49 ± 0.03	0.98
No. 6 (1.9)	0.9 ± 0.2	0.81	1.62 ± 0.01	0.95	nd	/	0.63 ± 0.08	2.3 ± 0.1	0.96	5.16 ± 0.06	0.93
No. 7 (0.72)	1.0 ± 0.5	0.95	3.60 ± 0.03	0.93	nd	/	0.61 ± 0.02	10.5 ± 0.3	0.98	3.54 ± 0.03	0.95
Mean	1.2 ± 0.4		2.7 ± 0.6		4 ± 1		0.5 ± 0.2	14 ± 11		2.5 ± 2	

<sup>a</sup>Under the inhalation sequence of air-carbogen-air-oxygen-air.

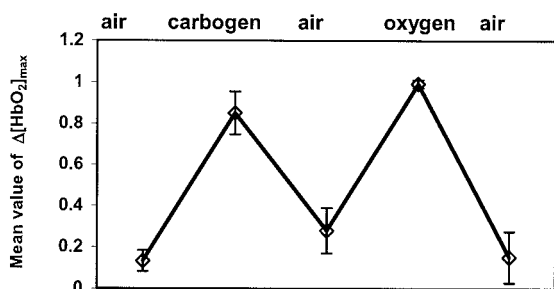
<sup>b</sup>nd, not determined.



(a)



(b)



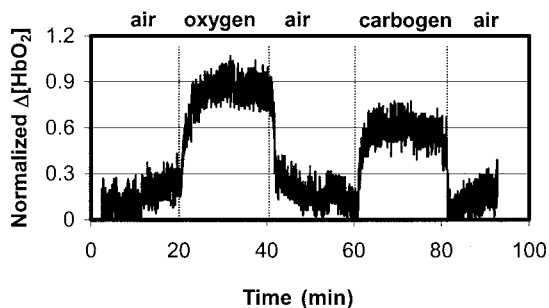
(c)

Fig. 4. (a) Time course of changes in tumor vascular  $\Delta[\text{HbO}_2]$  for a representative 13762NF breast tumor from Group 1 (No. 2, 3.0  $\text{cm}^3$ ) with respect to altering inhaled gas. (b) Respective curve fits for the carbogen and oxygen interventions. (c) Average maximum values of normalized  $\Delta[\text{HbO}_2]$  for the seven breast tumors in Group 1.

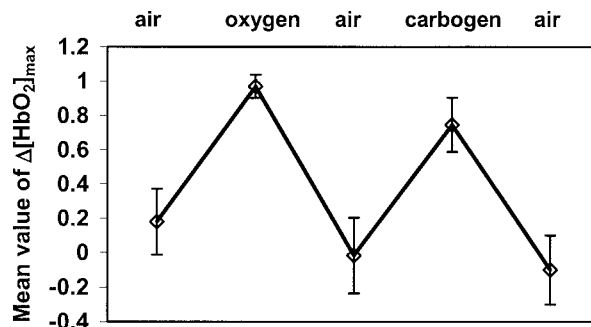
secutive interventions [Fig. 5(c)]. In this case, non-normalized data are shown for specific comparison of the absolute  $\Delta[\text{HbO}_2]_{\text{max}}$  produced by oxygen and carbogen for each of the tumors.

### C. Tumor $\text{pO}_2$

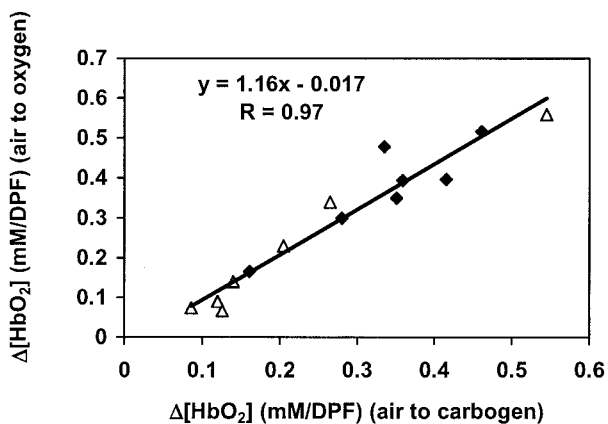
The FOXY  $\text{pO}_2$  probes generally indicated distinct heterogeneity in  $\text{pO}_2$ . Moreover, response to the hy-



(a)



(b)



(c)

Fig. 5. (a) Dynamic changes in tumor vascular  $\Delta[\text{HbO}_2]$  for a representative 13762NF breast tumor from Group 2 (No. 9, 2.6  $\text{cm}^3$ ) with gas-inhalation sequence reversed compared with Group 1. (b) Average maximum values of normalized  $\Delta[\text{HbO}_2]$  for Group 2. Gas-inhalation sequence reversed compared with Group 1. (c) Correlation between maximum  $\Delta[\text{HbO}_2]$  achieved with carbogen inhalation versus that with oxygen ( $R = 0.97$ ):  $\blacklozenge$ , carbogen first;  $\triangle$ , oxygen first.

peroxic gas was diverse: those probes that indicated apparently well-oxygenated regions usually showed a large and rapid response, whereas those with lower baseline  $\text{pO}_2$  often showed little change [Fig. 6(a)]. The  $\text{pO}_2$  responses to the two interventions showed a highly consistent behavior at each individual location [Fig. 6(b)]. There was also a distinct correlation between the global NIR measurements and the mean  $\Delta\text{pO}_2$  (Fig. 7). Because of heterogeneity in regional  $\text{pO}_2$ , the standard deviations of the mean  $\text{pO}_2$  values were large.

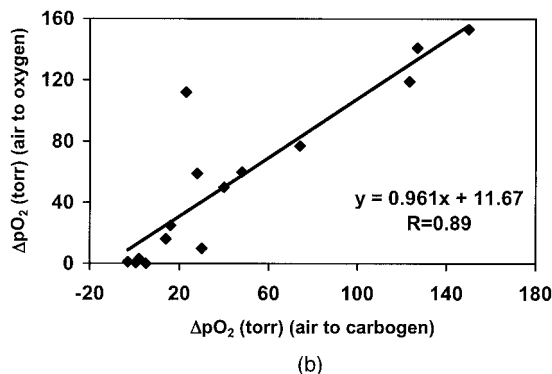
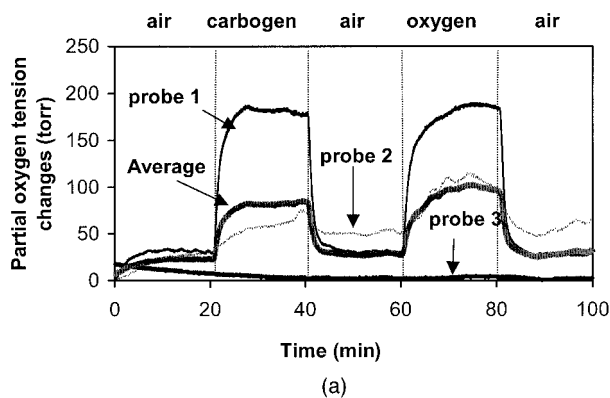


Fig. 6. (a) Time profiles of tumor  $\Delta pO_2$ , measured with the three channels of the FOXY fiber-optic, oxygen-sensing system with respect to different gas inhalations for breast tumor No. 3 ( $4.6 \text{ cm}^3$ ). The mean signal for the three channels was calculated and is plotted by the thicker trace. (b) Correlation between  $\Delta pO_2$  at individual locations in the tumors in response to carbogen or oxygen for the five tumors in Group 1 ( $R > 0.8$ ).

#### 4. Discussion

In this study, we have simultaneously measured the arterial  $\text{SaO}_2$ , the global changes in the  $\Delta[\text{HbO}_2]$  of tumor vasculature, and the regional changes in the  $\Delta pO_2$  of tumor tissue, in response to hyperoxic (i.e., carbogen and oxygen) gas interventions with a pulse oximeter, an NIRS system and a multichannel, fiber-optic, oxygen-sensing system, respectively. All three oxygen-sensitive indicators displayed similar

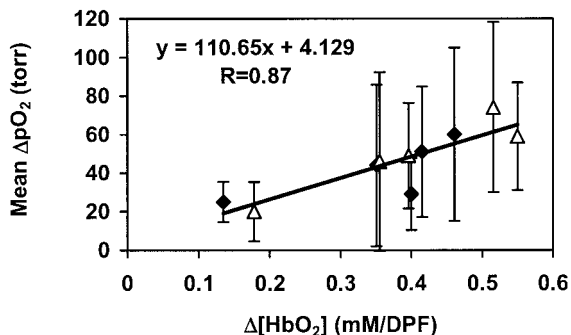


Fig. 7. Correlation between mean  $\Delta pO_2$  and  $\Delta[\text{HbO}_2]$  for the five breast tumors ( $R > 0.86$ ):  $\blacklozenge$ , transition from air to carbogen;  $\blacktriangle$ , transition from air to oxygen.

dynamic tendency in response to carbogen intervention (Fig. 2).

The simultaneous measurements demonstrate the compatibility of the NIRS system with the FOXY fiber-optic oxygen-sensing system, without interference. Both systems are relatively inexpensive and provide real-time measurements, but the multichannel FOXY fiber-optic system monitors  $\Delta pO_2$  in specific locations, whereas the NIRS system provides global measurements. Whether  $\Delta\text{HbO}_2$  determined with this methodology will be a clinically useful predictor for tumor response to oxygen-dependent interventions and therapies remains to be determined. However, it is established that measurements of  $pO_2$  have prognostic value in the clinic<sup>18,20</sup> so that correlations between  $pO_2$  and NIR measurements would be very important.

We have previously applied a polarographic oxygen electrode simultaneously with NIR.<sup>25</sup> However, that study provided only a single local  $pO_2$  value, and in some cases correlations with global NIR measurements were very poor. The optical fiber system used here allows multiple locations to be interrogated simultaneously. The device can be expanded to many channels, but our system uses four channels. Unfortunately, probes are fragile, and the oxygen-sensitive coating on the tips is readily damaged. Thus, we only had three probes available for this study. Indeed, fiber-optic probe fragility is a well-recognized problem, and our previous experience with the more expensive OxyLite system was also restricted to three channels owing to probe damage.<sup>26</sup>

The FOXY system ( $\sim \$13\text{k}$ ) is much less expensive than the OxyLite ( $\sim \$48\text{k}$ ), and its mode of action is also simpler, detecting fluorescent signal intensity rather than fluorescence lifetime. It seems capable of measuring  $pO_2$  across the whole range of atmospheric oxygen tensions (0–760 Torr), whereas the OxyLite is restricted and becomes very insensitive above approximately 100 Torr. However, our experience shows that although the FOXY system provides precise measurements of  $\Delta pO_2$ , absolute values of  $pO_2$  may not be reliable. We continue to perform validation experiments. By contrast, the OxyLite system seems to give very accurate  $pO_2$  values.

Our experience shows that the FOXY probes are much easier to use than electrodes, particularly, in terms of calibration and stability. Since the probes are fragile, we insert them into tumors through a fine needle (25 gauge), which readily punctures the surrounding skin and penetrates tough fibrous tissues. The needle is then backed up from the tip to facilitate measurements. The probes often require a few minutes to settle at a stable baseline value, but then show good baseline stability and rapid response to interventions [Figs. 2 and 6(a)]. They are easily moved within the tumor to locate regions, presenting a particular  $pO_2$  of interest, e.g. hypoxic or well oxygenated. In the search for appropriate locations, probes are moved forward to interrogate fresh tissues rather than in reverse, since blood may pool in the tracks owing to vascular damage. However, we observe

minimal bleeding on removal of the probes from the tumors.

We have found no interference between the NIR and FOXY instruments, although any tumor motion associated with moving the fiber probes can alter the optical contact of the NIR optrodes, and thus, alter apparent  $\Delta\text{HbO}_2$ . Thus, baseline  $\Delta\text{HbO}_2$  is determined once the fiber probes are situated. New fiber-optic probes of the FOXY system have a thick coating of fluorescent gel and a black covering, but this wears with use and gradually allows reception of the NIR light. Since the LEDs of the two systems operate at very different wavelengths, viz. 475 versus 760 nm, there is no interference for detection. The detection of local NIR light by the FOXY probe opens the exciting possibility of detecting regional hemoglobin oxygen saturation. We believe the FOXY optical probes could be moved within the tumor to map the distribution and path of the transmitted NIR light, helping to explore and validate the optical characteristics of the tumor. This can simultaneously provide a correlation between local  $\Delta\text{HbO}_2$  and  $\Delta\text{pO}_2$ .

In this study, we have examined a much larger group of rats than previously.<sup>16,25</sup> We have now shown rigorously that the two hyperoxic gases induce similar changes in vascular oxygenation (NIR) and regional tissue  $\text{pO}_2$  (FOXY) in this type of rat breast tumor. These data are consistent with our previous observations using  $^{19}\text{F}$  NMR imaging (FREDOM)<sup>33</sup> in this tumor type and also in rat prostate tumors.<sup>34,35</sup> If the two gases are indeed equivalent in terms of manipulation of tumor oxygenation, it could have great therapeutic benefit since the popular carbogen, which is in use in clinical trials,<sup>36</sup> can cause respiratory discomfort.

The current data show that  $\Delta\text{HbO}_2$  and  $\Delta\text{pO}_2$  are correlated (Fig. 7), and thus, such noninvasive observations could have value in the clinic. The major deficiency in our current NIR approach is lack of spatial discrimination, and thus efforts to implement NIR imaging will be of great value. It will also be interesting to correlate other measurements, such as blood-oxygen-level-dependent (BOLD) proton magnetic resonance imaging, which provide high spatial resolution, but which are sensitive to vascular flow and volume as well as oxygenation.<sup>37</sup>

The biphasic response of  $\Delta\text{HbO}_2$  to carbogen is intriguing, and we believe it represents the distinct vascular compartments of arterioles (high flow) and capillaries. However, the change to monophasic behavior, when carbogen is administered second, requires further exploration; in the future, we propose to test various concentrations of oxygen and carbon dioxide and air to separate the components of the response. The carbogen dioxide component of carbogen is known to be vasoactive; however, the specific effects may depend on tumor type, site of growth, and other factors.<sup>9,38</sup>

In terms of vascular oxygen delivery, the data in Table 1 reveal the progressive movement of oxygen:  $t_d(\text{SaO}_2) < t_d(\Delta[\text{HbO}_2]) < t_d(\Delta\text{pO}_2)$ . As expected, switching to hyperoxic gas caused the systemic arte-

rial  $\text{SaO}_2$  to increase, as a result of the immediate combination of deoxyhemoglobin with oxygen. The highly oxygenated blood circulated in the systemic vasculature of the rats (including the capillary bed of the tumor tissue), resulting in a delayed increase in  $[\text{HbO}_2]$  in the tumor vasculature, and led to an unloading of oxygen to the tumor tissue. For the biexponential model of  $\Delta[\text{HbO}_2]$ , the fast component has a similar time constant to the  $\text{SaO}_2$  measured with the pulse oximeter on the hind leg, strongly suggesting that it represents arteriolar oxygenation in the tumor. In this study, tumor volumes do not show any direct relation with time constants or changes of amplitude in response to hyperoxic gas interventions.

It is increasingly evident that oxygen and hypoxia play important roles in tumor development and response to therapy.<sup>18</sup> NIR offers an attractive non-invasive means of investigating tumor oxygenation, particularly in terms of dynamic response to interventions, but we had previously shown a potential mismatch between global  $\Delta\text{HbO}_2$  and local  $\Delta\text{pO}_2$ .<sup>25</sup> The data presented here indicate a correlation between the global NIR measurements and mean  $\text{pO}_2$  values with even as few as three representative locations per tumor. This does suggest that it will be important to develop regional NIR measurements and that even relatively crude mapping could reveal heterogeneity. In the meantime, we believe these studies provide further evidence for the value of NIRS to explore tumor physiology.

This study was supported in part by the Department of Defense Breast Cancer Research grants BC000833 (YG) and BC990287 (HL), and NIH RO1 CA79515 (RPM) and RO1 supplement CA79515-S (VB). We are grateful to Mengna Xia and Dawen Zhao for their assistance with data processing. We gratefully acknowledge Weina Cui for helpful discussions.

## References

1. R. S. Bush, R. D. T. Jenkin, W. E. C. Allt, F. A. Beale, A. J. Dembo, and J. F. Pringle, "Definitive evidence for hypoxic cells influencing cure in cancer therapy," *Br. J. Cancer* **37**(suppl 3), 302–306 (1978).
2. E. J. Hall, *Radiobiology for the Radiologist*, 4th ed. (Lippincott, Philadelphia, Pa., 1994).
3. M. Nordmark and J. Overgaard, "A confirmatory prognostic study on oxygenation status and loco-regional control in advanced head and neck squamous cell carcinoma treated by radiation therapy," *Radiother. Oncol.* **57**, 39–43 (2000).
4. O. Thews, D. K. Kelleher, and P. Vaupel, "Erythropoietin restores the anemia-induced reduction in cyclophosphamide cytotoxicity in rat tumors," *Cancer Res.* **61**, 1358–1361 (2001).
5. J. H. A. M. Kaanders, L. A. M. Pop, H. A. M. Marres, R. W. M. van der Maazen, A. J. van der Kogel, and W. A. J. van Daal, "Radiotherapy with carbogen breathing and nicotinamide in head and neck cancer: feasibility and toxicity," *Radiother. Oncol.* **37**, 190–198 (1995).
6. M. I. Saunders, P. J. Hoskin, and K. Pigott, "Accelerated radiotherapy, carbogen and nicotinamide (ARCON) in locally advanced head and neck cancer: a feasibility study," *Radiother. Oncol.* **45**, 159–166 (1997).
7. J. A. Kruuv, W. R. Inch, and J. A. McCredie, "Blood flow and

- oxygenation of tumors in mice. I. Effects of breathing gases containing carbon dioxide at atmospheric pressure," *Cancer*. **20**, 51–59 (1967).
8. J. Overgaard and M. R. Horsman, "Modification of hypoxia-induced radioresistance in tumors by the use of oxygen and sensitizers," *Semin. Radiat. Oncol.* **6**, 10–21 (1996).
  9. P. Vaupel, D. K. Kelleher, and O. Thews, "Modulation of tumor oxygenation," *Int. J. Radiat. Oncol. Bio. Phys.* **42**, 843–848 (1998).
  10. S. Dische, "What we learnt from hyperbaric oxygen?" *Radiother. Oncol.* **20**(Suppl.), 71–74 (1991).
  11. S. Dische, M. I. Saunders, and R. Sealy, "Carcinoma of the cervix and the use of hyperbaric oxygen with radiotherapy: a report of a randomized controlled trial," *Radiother. Oncol.* **53**, 93–98 (1999).
  12. V. M. Laurence, R. Ward, I. F. Dennis, and N. M. Bleehen, "Carbogen breathing with nicotinamide improves the oxygen status of tumors in patients," *Br. J. Cancer* **72**, 198–205 (1995).
  13. L. Martin, E. Lartigau, and P. Weeger, "Changes in the oxygenation of head and neck tumors during carbogen breathing," *Radiother. Oncol.* **27**, 123–130 (1993).
  14. H. B. Stone, J. M. Brown, T. Phillips, and R. M. Sutherland, "Oxygen in human tumors: correlations between methods of measurement and response to therapy," *Radiat. Res.* **136**, 422–434 (1993).
  15. E. L. Hull, D. L. Conover, and T. H. Foster, "Carbogen induced changes in rat mammary tumor oxygenation reported by near infrared spectroscopy," *Br. J. Cancer* **79**, 1709–1716 (1999).
  16. H. Liu, Y. Song, K. L. Worden, X. Jiang, A. Constantinescu, and R. P. Mason, "Noninvasive investigation of blood oxygenation dynamics of tumors by near-infrared spectroscopy," *Appl. Opt.* **39**, 5231–5243 (2000).
  17. R. G. Steen, K. Kitagishi, and K. Morgan, "*In vivo* measurement of tumor blood oxygenation by near-infrared spectroscopy: immediate effects of pentobarbital overdose or carmustine treatment," *J. Neuro-Oncol.* **22**, 209–220 (1994).
  18. M. Höckel and P. Vaupel, "Tumor hypoxia: definitions and current clinical, biologic, and molecular aspects," *J. Natl. Cancer Inst.* **93**, 266–276 (2001).
  19. L. Gray, A. Conger, M. Ebert, S. Hornsey, and O. Scott, "The concentration of oxygen dissolved in tissues at time of irradiation as a factor in radio-therapy," *Br. J. Radiol.* **26**, 638–648 (1953).
  20. A. W. Fyles, M. Milosevic, R. Wong, M. C. Kavanagh, M. Pintile, A. Sun, W. Chapman, W. Levin, L. Manchul, T. J. Keane, and R. P. Hill, "Oxygenation predicts radiation response and survival in patients with cervix cancer," *Radiother. Oncol.* **48**, 149–156 (1998).
  21. D. Zhao, A. Constantinescu, E. W. Hahn, and R. P. Mason, "Measurement of tumor oxygen dynamics predicts beneficial adjuvant intervention for radiotherapy in Dunning prostate R3327-HI tumors," *Radiat. Res.* (to be published) (2003).
  22. C. Song, I. Lee, T. Hasegawa, J. Rhee, and S. Levitt, "Increase in pO<sub>2</sub> and radiosensitivity of tumors by Fluosol and carbogen," *Cancer Res.* **47**, 442–446 (1987).
  23. D. Cater and I. Silver, "Quantitative measurements of oxygen tension in normal tissues and in the tumors of patients before and after radiotherapy," *Acta Radiol.* **53**, 233–256 (1960).
  24. D. Zhao, A. Constantinescu, E. W. Hahn, and R. P. Mason, "Differential oxygen dynamics in two diverse Dunning prostate R3327 rat tumor sublines (MAT-Lu and HI) with respect to growth and respiratory challenge," *Int. J. Radiat. Oncol. Biol. Phys.* **53**, 744–756 (2002).
  25. J. G. Kim, Y. Song, D. Zhao, A. Constantinescu, R. P. Mason, and H. Liu, "Interplay of tumor vascular oxygenation and pO<sub>2</sub> in tumors using NIRS, <sup>19</sup>F MR pO<sub>2</sub> mapping, and pO<sub>2</sub> needle electrode," *J. Biomed. Optics* **8**, 53–62 (2003).
  26. D. Zhao, A. Constantinescu, E. W. Hahn, and R. P. Mason, "Tumor oxygen dynamics with respect to growth and respiratory challenge: investigation of the Dunning prostate R3327-HI tumor," *Radiat. Res.* **156**, 510–520 (2001).
  27. J. Bussink, J. H. A. M. Kaanders, A. M. Strik, B. Vojnovic, and A. J. van der Kogel, "Optical sensor-based oxygen tension measurements correspond with hypoxia marker binding in three human tumor xenograft lines," *Radiat. Res.* **154**, 547–555 (2000).
  28. J. R. Griffiths, "The OxyLite: a fibre-optic oxygen sensor," *Br. J. Radiol.* **72**, 627–630 (1999).
  29. Y. Gu, Z. Qian, J. Chen, D. Blessington, N. Ramanujam, and B. Chance, "High resolution three dimensional scanning optical image system for intrinsic and extrinsic contrast agents in tissue," *Rev. Sci. Instrum.* **73**, 172–178 (2002).
  30. Ocean Optics Inc., Dunedin, Fla., March 2003. <http://www.oceanoptics.com/products/foxsystem.asp>
  31. C. B. Allen, B. K. Schneider, and C. J. White, "Limitations to oxygen diffusion in *in vitro* cell exposure systems in hyperoxia and hypoxia," *Am. J. Physiol. Lung Cell Molec. Physiol.* **281**, L1021–L1027 (2001).
  32. E. W. Hahn, P. Peschke, R. P. Mason, E. E. Babcock, and P. P. Antich, "Isolated tumor growth in a surgically formed skin pedicle in the rat: a new tumor model for NMR studies," *Magn. Reson. Imaging* **11**, 1007–1017 (1993).
  33. Y. Song, A. Constantinescu, and R. P. Mason, "Dynamic breast tumor oximetry: the development of prognostic radiology," *Technol. Cancer Res. Treat.* **1**, 1–8 (2002).
  34. S. Hunjan, D. Zhao, A. Constantinescu, E. W. Hahn, P. P. Antich, and R. P. Mason, "Tumor oximetry: demonstration of an enhanced dynamic mapping procedure using Fluorine-19 echo planar magnetic resonance imaging in the Dunning prostate R3327-AT1 rat tumor," *Int. J. Radiat. Oncol. Biol. Phys.* **49**, 1097–1108 (2001).
  35. D. Zhao, A. Constantinescu, L. Jiang, E. W. Hahn, and R. P. Mason, "Prognostic radiology: quantitative assessment of tumor oxygen dynamics by MRI," *Am. J. Clin. Oncol.* **24**, 462–466 (2001).
  36. J. H. Kaanders, J. Bussink, and van der A. J. Kogel, "ARCON: a novel biology-based approach in radiotherapy," *Lancet Oncol.* **3**, 728–737 (2002).
  37. F. A. Howe, S. P. Robinson, L. M. Rodrigues, and J. R. Griffiths, "Flow and oxygenation dependent (FLOOD) contrast MR imaging to monitor the response of rat tumors to carbogen breathing," *Magn. Reson. Imaging* **17**, 1307–1318 (1999).
  38. T. J. Dunn, R. D. Braun, W. E. Rhemus, G. L. Rosner, T. W. Secomb, G. M. Tozer, D. J. Chaplin, and M. W. Dewhirst, "The effects of hyperoxic and hypercarbic gases on tumour blood flow," *Br. J. Cancer* **80**, 117–126 (1999).